

The Effect of Symmetry Breaking in Coupled Cavity Photonic Crystal Waveguide on Dispersion Characteristics

Hasan Oguz¹, Zekeriya Mehmet Yuksel¹, Ozgur Onder Karakilinc^{2,*},
Halil Berberoglu³, Mirbek Turduev⁴, Sevgi Ozdemir Kart¹, Muzaffer Adak¹

¹ Department of Physics, Faculty of Science,

Pamukkale University, 20160 Pamukkale, Denizli, Turkey

²Department of Electric Electronic Engineering, Faculty of Engineering,

Pamukkale University, 20160 Pamukkale, Denizli, Turkey

³ Department of Physics, Polatli Faculty of Science and Letters,

Ankara Hacı Bayram Veli University, 06900 Polatli, Ankara, Turkey

⁴ Electrical and Electronics Engineering, Faculty of Engineering,

Kyrgyz-Turkish Manas University, Bishkek, Chuy, 720038 Kyrgyz Republic

Abstract

In this study, we explore the effect of integrated auxiliary rods at varying angles to the primary cavity rod on the dispersion characteristics of the photonic crystal coupled cavity waveguide (PC CCW). Here, it is intended to break the symmetry of the cavity region by introducing auxiliary rods which gives the degree of freedom for tuning effective index of the PC waveguide. Furthermore, rotational angle variations of auxiliary rods reveal slow light operation of the PC CCW where the group index is maximized and group velocity dispersion, as well as the third-order dispersion, are minimized. In addition, auxiliary rods with a broken symmetry increase not only group index but also operating bandwidth and accordingly increase group bandwidth product by 675%. Leveraging these results, we demonstrate effective rainbow trapping by manipulating the auxiliary rod angles in photonic crystal coupled cavity waveguides. Our results have encouraging implications for optical buffering, multiplexing, demultiplexing, advanced time-domain and spatial signal processing.

*okarakilinc@pau.edu.tr

Keywords: Photonic crystal, slow light, symmetry reduction, coupled cavity waveguide, rainbow trapping.

1 Introduction

Cavity structures hold significant importance in photonics, offering versatile functionalities such as optical filtering, modulation, buffering, delaying and switching within nanophotonic integrated devices and networks [1–9]. Coupled cavity waveguide (CCW) photonic crystal (PC) structures, which exploit the slow light (SL) effect with the low group velocity phenomena, emerge as promising avenues for enhancing light-matter interactions in various photonic applications [7–11]. These CCW PC structures, owing to their compatibility with silicon-on-insulator devices, optical delay lines and electrically integrated components, as well as their compact sizes, offer unique advantages in the realization of photonic integrated circuits [10].

The SL phenomenon is one of the core concepts in photonic crystals (PCs) and can be obtained in the flat regions of dispersion curves, which enables the tuning of optical properties [12, 13]. It is also crucial in realizing optical delay lines, optical buffers, and wavelength demultiplexing devices, among others [7, 14–18]. The SL effect can be tuned and enhanced by introducing line defects or manipulating structural defects such as the radius of rods/holes and the shapes of adjacent rows in PC waveguides [19–21]. Additionally, it is known that low-symmetry PC structures can be exploited to enhance optical properties within the SL region [19, 22–26]. Furthermore, the sensitivity of cavity behavior to minor distortions in their geometry presents a powerful tool for optimizing cavity parameters [24, 27]. It is important to note that cavities can also be exploited to demultiplex incoming signals with fine-tuned coupling parameters [28].

Another application of SL is the rainbow trapping (RT) effect [29]. The RT phenomenon involves the temporary trapping of electromagnetic waves with different wavelengths at distinct spatial positions. This effect is primarily attributed to spatial dispersion [30]. The RT effect can be achieved using graded-index PC structures, tapered PC structures, metallic gratings, chirped and topologically modified PCs, and metamaterials [31–37]. With the aid of a coupler, point defect, or tapering mechanism, this effect can be implemented in photonic device structures [36, 38]. These structures can be utilized in various applications such as optical switching, multiplexing, demultiplexing, and many other optical communication and information devices [26, 36–38]. The adaptability of these structures in photonic devices is pivotal, offering significant enhancements in the efficiency and performance of optical systems.

In this study, to the best of our knowledge, we present the design of rainbow trapping by utilizing the low-symmetry effect in the cavity, rather than in the entire structure, by adding auxiliary rods for the first time. It is important to note that we achieved the RT

effect by varying the angles of the auxiliary rods and combining them through symmetry breaking, without tapering or grading the PC structure. Our methods are based on plane wave expansion (PWE) via MPB and finite-difference time-domain (FDTD) via Lumerical.

2 Design Approach and Numerical Analysis of Coupled Cavity PC Waveguide with Symmetry Breaking

In this study, we present a detailed exploration of the impacts of symmetry reduction on the dispersion curves of waveguides exhibiting the SL effect. We employ both the plane wave expansion (PWE) and finite-difference time-domain (FDTD) methods for frequency and time domain analysis of the photonic crystal (PC) structures to reveal the SL effect and apply it to the rainbow trapping application, respectively [39–41]. The combination of these approaches provides a comprehensive exploration of the influence of symmetry reduction on SL properties in both the time and spectral domains. Throughout the study, freely available software MPB (based on the PWE method) is used for calculating dispersion characteristics, while Ansys Lumerical FDTD is employed for time-domain simulations. The PWE method provides frequency-domain analysis, and the FDTD simulations allow for time-domain analysis, enabling a thorough investigation of the slow light effect and rainbow trapping applications.

The photonic band diagrams of both primitive and supercell PC structures are calculated using the PWE method, and by introducing line and cavity defects, we generate the desired guided modes. Fig. 1a presents the schematic view of the PC coupled cavity waveguide (CCW) structure. This structure comprises square lattice dielectric rods with a radius of $0.20a$ distributed in an air medium. The distance between the centers of adjacent rods is set to the lattice constant a . We design a cavity waveguide structure by integrating dielectric rods with a radius of $0.35a$ into the W1 PC waveguide. This configuration gives rise to prominent defect modes within the first band gap of the photonic band structure, as shown in Fig. 1b. The calculated mode profile of the gap-guided transverse magnetic (TM) mode at $k = 0.25(2\pi/a)$ is also presented in Fig. 1c.

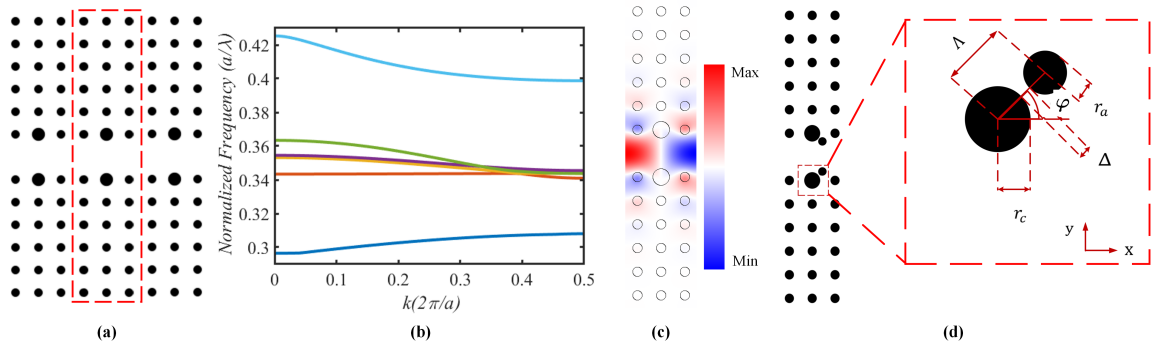


Fig. 1: (a) The schematic view of the PC CCW structure with dielectric rods having radii of $r = 0.2a$ and the dielectric constant of $\epsilon = 9.8$. Here the enlarged rods having radii of $r_c = 0.35a$ act as cavity regions, where a is the lattice constant. (b) Multi-band TM polarization defect modes of the cavity structure without auxiliary rods in the supercell structure. (c) TM polarized E_z Mod profile picture for 3rd band mode with TM polarization. (d) The supercell of low-symmetry cavity structure with introduced auxiliary rod. Cavity parameters; r_c and r_a are the cavity and the auxiliary rod radii, respectively, φ and Δ are the rotation angle of the auxiliary rod and the distance between the cavity and the auxiliary rod, respectively.

We propose a CCW design by replicating a $3a$ wide cavity supercell across the W1 waveguide and introducing symmetry reduction via auxiliary rod, as seen in Fig. 1d. The supercell of the low-symmetry cavity structure, with the introduced auxiliary rods and corresponding opto-geometrical parameters, is presented as an inset in the same figure plot. As shown in Fig. 1d, symmetry reduction is introduced in the cavity region to analyze the spectral effects of locally generated symmetry breaking on the performance of SL effect. In this regard, the band structures of symmetry-reduced PC CCW are calculated and presented in Fig. 2 for specifically selected auxiliary rods radius of $r_a = 0.14a$ and rotation angles of auxiliary rods of $\varphi = [15^\circ, 30^\circ, 45^\circ, 60^\circ, 75^\circ, 90^\circ]$ as shown in Figs. 2a-2f, respectively. Additionally, the radius of the cavity and the distance between the cavity and the auxiliary rod are set to $r_c = 0.35a$ and $\Delta = 0.10a$, respectively.

The band diagrams in Figs. 2a-2f, illustrate the critical effect of rotation angle φ on the band structure. As φ increases from 15° to 90° , the 2nd band shifts to the lower frequencies, while the 3rd and 4th bands move closer to the 5th band. At $\varphi = 90^\circ$, all three bands are closely located around normalized frequencies of $a/\lambda = 0.35$ and $a/\lambda = 0.36$. This indicates that the rotation of the auxiliary rods from 15° to 90° increases the effective index n_{eff} of the CCW in the propagation direction. The n_{eff} characterizes the guided modes in the waveguide, representing an equivalent refractive index that accounts for the confinement and propagation characteristics within the waveguide [42]. This change in n_{eff} is prominent in the 2nd band until $\varphi = 60^\circ$ and remains constant up to 90° . However, the 3rd band shows a clear separation from the 2nd band and exhibits unique dispersion

characteristics. The 3rd band decreases in frequency as φ increases from 15° to 60°, followed by an increase from 60° to 90°. As described in Figs. 2a-2d, the rotation angle of the auxiliary rods significantly alters the frequency bands of interest, paving the way for optical applications where fine-tuning the frequency response of the PC CCW is essential.

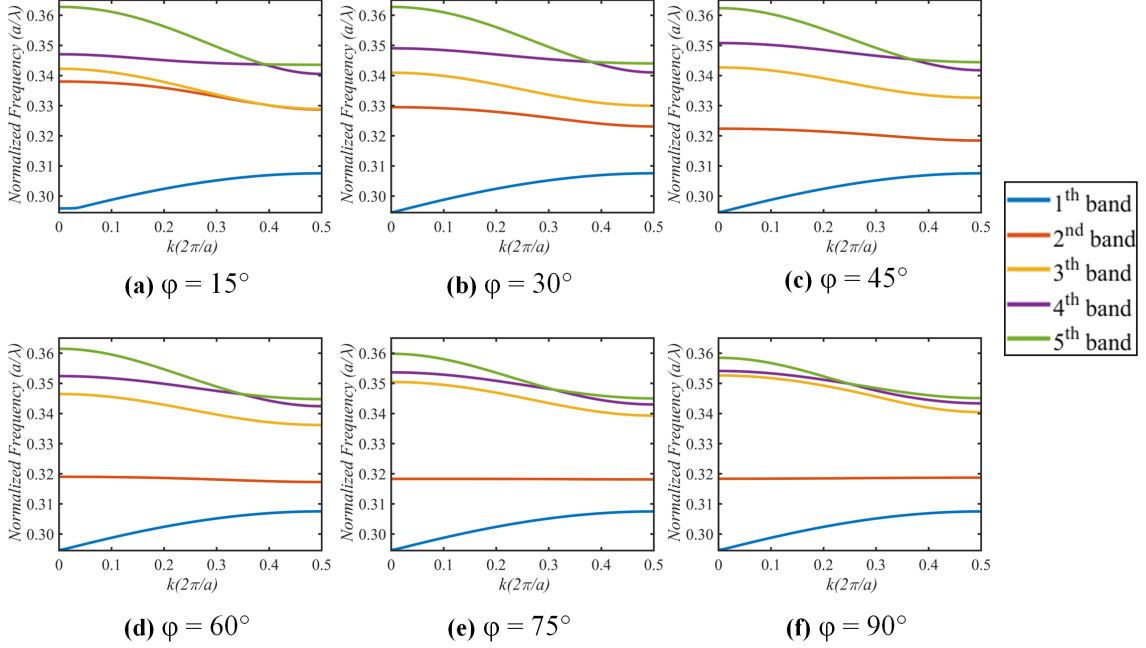


Fig. 2: The band structure of low-symmetry cavity structure with the auxiliary rods of radius $r_a = 0.14a$ at the angles of (a) $\varphi = 15^\circ$, (b) $\varphi = 30^\circ$, (c) $\varphi = 45^\circ$, (d) $\varphi = 60^\circ$, (e) $\varphi = 75^\circ$ and (f) $\varphi = 90^\circ$. The radius of cavity and the distance between the cavity and the auxiliary rod are taken as $r_c = 0.35a$ and $\Delta = 0.10a$, respectively.

While the 2nd band shows a flat profile, the response to symmetry reduction is limited, remaining unaffected by angle alterations between 60° and 90°. Additionally, the 4th and 5th bands are closely intertwined, showing no clear separation. This makes the 3rd band the most suitable candidate for exploitation. As seen in Figs. 2a-2d, while the radius of the auxiliary rod is kept constant, the rotation angle is varied. It is also important to assess the effect of auxiliary rod radii on the frequency band of interest. In Fig. 3, the impact of varying the auxiliary rod radius on the evolution of the frequency band is presented. By tuning the radius of the auxiliary rod r_a from $0.10a$ to $0.17a$ and adjusting the rotation angle from 15° to 90°, one can observe how the 3rd frequency band is maintained, as shown in Figs. 3a-3f. The separation distance is fixed at $\Delta = 0.10a$. The 3rd band exhibits a positive correlation between r_a and frequency. However, as φ increases, this effect diminishes, and the influence of r_a on frequency becomes negligible after $\varphi = 75^\circ$.

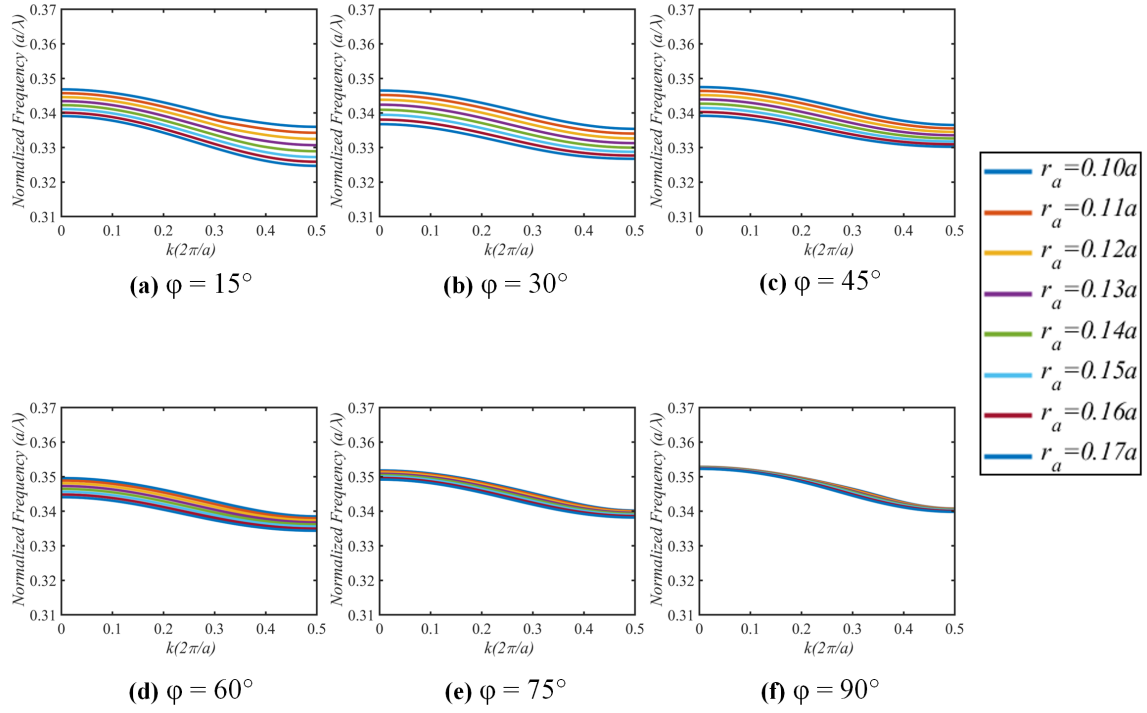


Fig. 3: The variation of normalized frequency of the 3rd band with the radius of auxiliary rod ranging between $r_a = 0.10a - 0.17a$ for the auxiliary rod angles of (a) $\varphi = 15^\circ$, (b) $\varphi = 30^\circ$, (c) $\varphi = 45^\circ$, (d) $\varphi = 60^\circ$, (e) $\varphi = 75^\circ$ and (f) $\varphi = 90^\circ$. The radius of cavity and the distance between cavity and auxiliary rod are taken as $r_c = 0.35a$ and $\Delta = 0.10a$, respectively.

Notably, the alteration in r_a provides a basis for refining the response characteristics of the structure. Additionally, we found that when the symmetry of the structure is reduced, angle adjustments can serve as an effective mechanism to tune the SL response, introducing another dimension of control in manipulating the SL properties of the system. This approach allows for precise control of SL parameters, such as n_g and GBP, with the desired frequency responses. As shown in Figs. 2 and 3, frequency bands exhibiting the SL effect and the effective dynamics of the targeted band modes can be achieved by introducing auxiliary rods with carefully chosen opto-geometrical parameters into the PC CCW. Based on the results presented in Fig. 3, the most effective auxiliary rod radius was determined to be $r_a = 0.14a$, considering the geometrical and fabrication limits of the proposed PC CCW.

The 1st band is independent of symmetry reduction, as is the 2nd band, although the latter exhibits SL characteristics, as mentioned earlier. There is a noticeable inclination in the φ angle beyond 60°. The 4th and 5th bands are intertwined, and this overlap increases with the φ angle, especially after 60°. Consequently, the 3rd band emerges as a promising operational candidate, offering the necessary bandwidth and SL characteristics. The band structure of the 3rd band for φ angles of 60° and 75° is shown in Fig. 4a.

To quantitatively analyze the SL effect, we exploited the slope information of the 3rd band mode to calculate the group index n_g and group velocity v_g , which are presented in Fig. 4b for rotation angles of $\varphi = 60^\circ$ and $\varphi = 75^\circ$. Here, the relationship $v_g = c/n_g = d\omega/dk$ is employed, where c represents the speed of light in a vacuum, ω is the angular frequency as normalized frequency $\omega(a/\lambda)$, and $k(2\pi/a)$ stands for the wave number.

Our research primarily focuses on conducting a detailed exploration of the impacts of symmetry reduction on the dispersion curves of waveguides. The main objective is to enhance the understanding of low-dispersion SL, characterized by low group velocity dispersion (GVD) [7]. This investigation utilizes a dual computational approach, incorporating both the PWE method and the FDTD method for frequency and time domain analysis of the PC structures, respectively [39–41]. The combination of these methods provides a comprehensive exploration of the influence of symmetry reduction on the properties of SL in both time and spectral domains. We calculated the photonic band diagrams of both primitive and supercell PC structures using the PWE method. By introducing line and cavity defects into the PC structure, we revealed the desired defect modes. From these defect modes, we derived the group index n_g and group velocity v_g , which are key parameters for understanding the light propagation characteristics of the model structure.

It is also crucial to analyze SL effect in terms of group velocity dispersion (GVD) and third-order dispersion (TOD) parameters. The GVD and TOD are the key parameters used to characterize SL phenomenon in the frequency domain quantitatively. GVD, characterized by $\partial^2\omega/\partial k^2$, dictates the propagation speeds of various frequency components of a light pulse through the medium. This is essential for optimizing the

characteristics of SL, making it crucial for broadening the operational bandwidth [8, 43–45]. On the other hand, TOD, represented by $\partial^3\omega/\partial k^3$, adds another layer of complexity as it influences the temporal shape of the propagating pulse. In dispersive media, TOD becomes significant, leading to either pulse broadening or compression depending on its sign and magnitude [43, 44, 46]. Another useful parameter for determining how effectively different frequency components of a light signal are spatially separated and slowed down is the group index bandwidth product (GBP), which can be formulated as $GBP = \langle n_g \rangle \frac{\Delta\omega}{\omega_0}$, where ω_0 is the midpoint frequency, $\Delta\omega$ is the bandwidth of the band, and $\langle n_g \rangle$ is the average group index, given by $\langle n_g \rangle = \frac{1}{\Delta\omega} \int_{\omega_0}^{\omega_0+\Delta\omega} n_g(\omega) d\omega$ [16]. High GBP values allow a wider range of frequencies to be effectively trapped with significant delay, facilitating advanced optical manipulations and signal processing techniques [2, 47]. The corresponding GVD and TOD values are presented in Fig. 4c for rotation angles of $\varphi = 60^\circ$ and $\varphi = 75^\circ$.

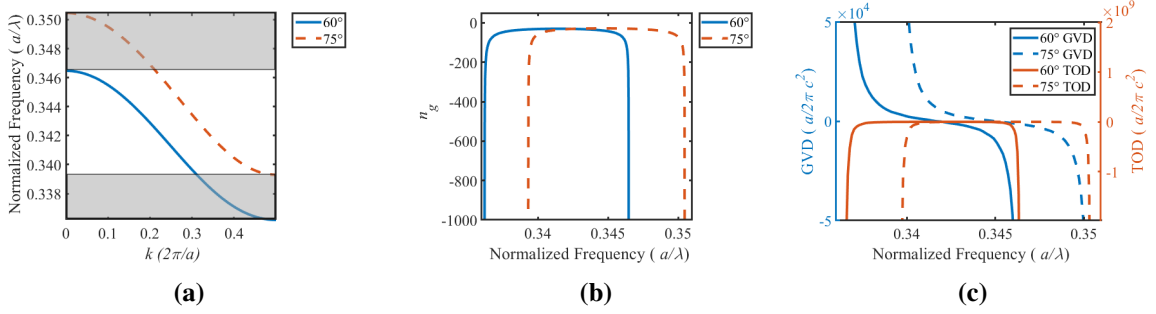


Fig. 4: (a) Band structure and (b) n_g , (c) GVD and TOD values of 3^{rd} band for auxillary rod angles φ of 60° and 75° structures showing mini-band gap.

From Fig. 4a, the structure creates a clear gap and a converging region, which can be effectively utilized for rainbow trapping. As discussed earlier, the frequency is closely tied to the φ angle. When reducing symmetry for the 3^{rd} band, there is an increase in frequency without disturbing the bandwidth and SL parameters, as shown in Table 1 and also observed in Fig. 4b. Interestingly, this stability extends to TOD and GVD, as seen in Fig. 4c, ensuring minimal pulse deformation while breaking symmetry. This characteristic can be particularly useful for designing RT-based devices.

3 Symmetry Breaking and Rainbow Trapping

While low-symmetry applied to the overall structure has been reported in the literature [26], the focus of our study is to investigate the effects of locally generated symmetry reduction in the cavity, specifically achieved by integrating an auxiliary rod at various

angles to the main cavity rod. We aim to leverage this approach to control SL, GBP, and transmission parameters. Our design adopts a square lattice configuration with a lattice constant a and rods of radius $r = 0.2a$, as shown in Fig. 1. This structure features a W1 waveguide created by removing a single row of rods. The supercell of the design is $3a$ wide. A cavity is formed in the supercell by modulating the rod radii of the mirror-symmetric middle rods to $r_c = 0.35a$. This design yields a primary bandgap in the normalized frequency range of $(0.30 - 0.40)a/\lambda$, with multiband guided modes appearing approximately within the range of $(0.34 - 0.37)a/\lambda$. We focus on achieving separation by adding low-symmetry alterations for RT, which produces defect modes exhibiting grouped behavior and degeneration, as shown in Fig. 1. The insights garnered from this study are expected to advance the understanding of structural effects on photonic characteristics, particularly in contexts requiring fine control over SL and GBP parameters with minimal symmetry perturbations.

Our study progresses by conducting PWE-based simulations to examine the effects of the asymmetrical angle of auxiliary rods on the optical properties of the RT model. We calculate the band structure and SL parameters, including n_g , v_g , GBP, GVD, and TOD. The structure of the supercell and the structural parameters of the RT model are shown in Fig. 1d. The SL parameters exhibit considerable fluctuations depending on the angle of the auxiliary rod. Notably, at certain angles, the group index is maximized while maintaining a relatively high GBP in the SL region. We then leverage the symmetry-breaking effect by combining two different auxiliary rod angles within the cavity to achieve RT with SL effect, creating mini-band gaps that can be effectively used for RT. As the angle of the auxiliary rods increases, the band frequency decreases, which is directly related to the symmetry reduction, as shown in Figs. 2a-2f. Specifically, as the angle between the cavity (located along the x -axis) and the auxiliary rod increases from 15° to 60° , both the cutoff frequency and center frequency ω_0 decrease significantly. This behavior has the potential to fine-tune the frequency response of the proposed structure.

The effect of the auxiliary rod angle on the band structure of the PC is most clearly observed in the first SL defect mode, where the auxiliary rod radius is $r_a = 0.14a$. This phenomenon manifests as a distinct separation of band modes, reaching a maximum at an angle of 90° , as depicted in Fig. 3. By modulating the radius r_a of the auxiliary rod within the range of $0.10a - 0.17a$ while keeping the separation distance constant at $\Delta = 0.10a$, we successfully improved the frequency response of the 3rd band, as shown in Figs. 3a-3f. Notably, this adjustment in r_a provides a foundation for refining the response characteristics of the structure. Additionally, we found that when the symmetry of the structure is reduced, angle adjustments can serve as a mechanism to tune the SL response, introducing an additional dimension of control over the SL properties of the system. In this way, we can control SL parameters such as n_g and GBP to achieve the desired frequency responses. Using these techniques, we achieved RT by combining different angle CCWs through symmetry breaking. A conspicuous separation of the band modes is particularly

evident when the auxiliary rod radius is $r_a = 0.14a$. This separation forms the basis of our RT efforts. As seen in Fig. 4a, this separation is most prominent around the 60° and 75° auxiliary rod angles, leading to a marked band gap that can be exploited for RT. Moreover, as seen in Fig. 4b, the SL effects are promising for any SL-based applications. Additionally, the relatively low GVD and TOD behaviors of the band, as observed in Fig. 4c, may be beneficial for light manipulation without disturbing the propagating wave shape, making them advantageous for RT applications.

Table 1 summarizes the results of GBP for the structure with $r_a = 0.14a$ auxiliary rods at the angles of $\varphi = 60^\circ$ and $\varphi = 75^\circ$ (Model B), along with a comparison of the results for the structure without auxiliary rods (Model A). The total trapping performance characteristics of the structure can be easily obtained from Fig. 4a. For the 3^{rd} band modes, the bandwidth and the midpoint frequency for trapping are calculated as $\Delta\omega = 0.0061a/\lambda$ and $\omega_0 = 0.3380a/\lambda$, respectively. Table 1 also includes information about the SL performance. Notably, there are significant increases in both $\Delta\omega$ and $\langle n_g \rangle$ when comparing Model A to Model B. Model B, with $\varphi = 60^\circ$ and $\varphi = 75^\circ$ angle values, exhibits a 50.07% and 32.67% increase in $\Delta\omega$, respectively. Similarly, the $\langle n_g \rangle$ values in Model B increase by 282.16% for $\varphi = 60^\circ$ and 1813.72% for $\varphi = 75^\circ$. The substantial differences in parameters for $\varphi = 60^\circ$ and $\varphi = 75^\circ$ are primarily due to the altered field distribution and mode coupling introduced by the different rotational angles of the auxiliary rods. These angles impact the photonic band structure, leading to distinct dispersion and bandwidth characteristics. Consequently, this configuration demonstrates enhanced SL properties and is suitable for broken symmetry RT applications.

Table 1: The midpoint frequency ω_0 , the bandwidth $\Delta\omega$, the average group index $\langle n_g \rangle$, the average group velocity $\langle v_g \rangle$ times light velocity in vacuum c , GBP for the 3^{rd} band mode of PC cavity without auxiliary rods (Model A) and with auxiliary rods at the angles of 60° and 75° (Model B). All the values are valid for the radius of auxiliary rods $r_a = 0.14a$.

Model	r_a	φ	$\omega_0 (a/\lambda)$	$\Delta\omega (a/\lambda)$	$\langle n_g \rangle$	$\langle v_g \rangle (c)$	GBP
A	—	—	0.353157000	0.010815	162.2441584	0.018918020	0.506709799
B	0.14	60°	0.341294000	0.016230	620.0413845	0.020572013	3.420130191
B	0.14	75°	0.345040969	0.014351	3104.8971230	0.022326015	3.425385380

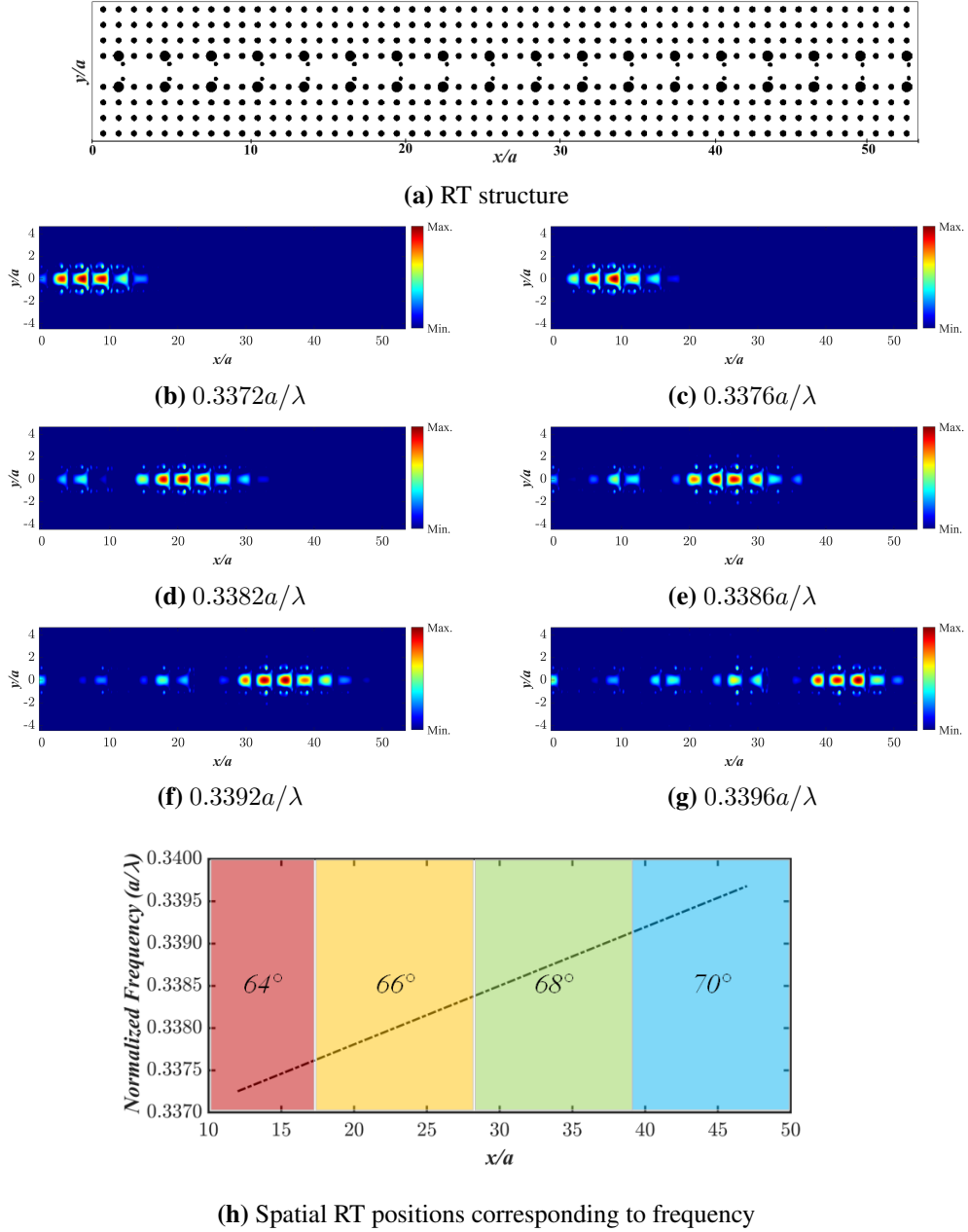


Fig. 5: The structure schematics and simulated electric field profiles for $\varphi = 60^\circ$ and $\varphi = 75^\circ$ with 2° gradual increase: (a) Top view of the photonic crystal coupled cavity waveguide with the starting auxiliary rods of the angle of $\varphi = 60^\circ$ and gradually increasing to $\varphi = 75^\circ$, E_z field intensities of (b) $\omega = 0.3372a/\lambda$, (c) $\omega = 0.3376a/\lambda$, (d) $\omega = 0.3382a/\lambda$, (e) $\omega = 0.3386a/\lambda$, (f) $\omega = 0.3392a/\lambda$, (g) $\omega = 0.3396a/\lambda$ and (h) spatial RT positions corresponding to frequency.

To achieve RT, we implemented the gradual increase in the φ angle with 2° increments, as shown in Fig. 5a. By introducing this lower symmetry alteration to the structure and gradually breaking symmetry, we successfully trapped light spatially within the normalized frequency range of $(0.3372 - 0.3396)a/\lambda$, with the E_z field profiles depicted in Figs. 5b-5g. These field profiles demonstrate that the localization is closely tied to frequency. The mini-band gap localization is also linked to the φ angle. Small structural alterations create a shifting mini-band gap, resulting in spatial localizations. The spatial localization of these frequencies is clearly shown in Fig. 5h, where the linear relationship between trapping position and frequency is evident. This structure is suitable for RT applications and can be implemented in any RT-based devices.

It is important to note that in the presented study, our primary objective was to demonstrate the concept of rainbow trapping through symmetry breaking in the waveguide defect region, rather than to fully develop and test the demultiplexing application. We conducted several simulations to demonstrate lateral light coupling at selected operating frequencies. While lateral channels were introduced at locations corresponding to light trapping, we acknowledge that these coupling mechanisms require further optimization for efficiency. It is important to clarify that the application of demultiplexing was beyond the scope of this initial study. Our results primarily aim to establish the foundational concept, paving the way for future studies to explore and optimize demultiplexing configurations in detail. Additionally, the robustness of the PC structure against imperfections cannot be overlooked, as it could indeed affect the practical application of the observed effects. In our simulations, we introduced variations to test the structure's sensitivity to imperfections. We found that $a \pm 5\%$ alteration in the radii of the dielectric rods and the spacing between them can cause shifts in the operating frequencies. Although these shifts can impact the dispersion properties, the fundamental concept of the light-trapping effect remains intact. This suggests that while exact precision is crucial for specific applications, the overall phenomenon of rainbow trapping can be robust under minor variations.

4 Conclusion

In this study, we explored the use of auxiliary rods to enhance SL parameters by introducing rotational symmetry reduction. Additionally, we achieved rainbow trapping (RT) by selectively applying low-symmetry modifications to the cavity structure in a novel way. Our technique offers clear advantages in device fabrication. The stable ω_0 and $\Delta\omega$ values achieved in this study make it feasible to design all-optically controlled delay lines for timing functions. The addition of auxiliary rods significantly improves both n_g and $\Delta\omega$ for the 3^{rd} band. For the proposed $\varphi = 60^\circ$ and $\varphi = 75^\circ$ structures, $\Delta\omega$ increased by 50.07% and 32.67%, respectively, while $\langle n_g \rangle$ increased by 282.16% and 1813.72%. These improvements notably enhance the GBP of the 3^{rd} band by 675%, underscoring the

potential of our findings. The wave propagation properties resulting from the gradual increase in broken symmetry from $\varphi = 60^\circ$ to $\varphi = 75^\circ$ present intriguing possibilities. The clear linear relationship between spatial RT positions and frequency may prove advantageous for any RT-based application. The entire structure exhibits relatively flat and low GVD and TOD values, offering opportunities for demultiplexer and multiplexer devices that maintain wave integrity while achieving SL effects and RT. This also opens up avenues for time-domain and spatial signal processing. For further controllability, the auxiliary rods could be manipulated by external means, such as mechanical or thermal interactions, enabling active control of light. This presents new opportunities for research in this domain and could lead to advancements in nanotechnology applications. The normalized frequency results could be adapted to various frequency bands, such as the terahertz region or the microwave domain. Overall, the use of auxiliary rods to achieve enhanced SL parameters with RT shows significant potential for the development of advanced optical devices with a wide range of applications.

5 Acknowledgement

This study was supported by the Scientific Research Coordination Unit of Pamukkale University under project number 2021FEBE041 and YÖK 100/2000 priority fields doctoral scholarship program. Also, we thank the anonymous referees for their guiding questions and criticisms.

References

- [1] E. Yablonovitch. Photonic band-gap structures. *J. Opt. Soc. Am. B*, 10(2):283–295, Feb 1993. doi: 10.1364/JOSAB.10.000283.
- [2] J. D. Joannopoulos, S. G. Johnson, J. N. Winn, and R. D. Meade. *Photonic Crystals: Molding the Flow of Light (Second Edition)*. Princeton University Press, 2 edition, 2008. ISBN 0691124566. doi: 10.2307/j.ctvc4gz9.
- [3] F. Xia, M. Rooks, L. Sekaric, and Y. Vlasov. Ultra-compact high order ring resonator filters using submicron silicon photonic wires for on-chip optical interconnects. *Opt. Express*, 15(19):11934–11941, Sep 2007. doi: 10.1364/OE.15.011934.
- [4] L. Zhang, M. Song, T. Wu, L. Zou, R. G. Beausoleil, and A. E. Willner. Embedded ring resonators for microphotonic applications. *Opt. Lett.*, 33(17):1978–1980, Sep 2008. doi: 10.1364/OL.33.001978.
- [5] M. Notomi, E. Kuramochi, and T. Tanabe. Large-scale arrays of ultrahigh-q coupled nanocavities. *Nature Photonics*, 2(12):741–747, Dec 2008. doi: 10.1038/nphoton.2008.226.
- [6] S. Xiao, M. H. Khan, H. Shen, and M. Qi. A highly compact third-order silicon microring add-drop filter with a very large free spectral range, a flat passband and a low delay dispersion. *Opt. Express*, 15(22):14765–14771, Oct 2007. doi: 10.1364/OE.15.014765.
- [7] S. Kubo, D. Mori, and T. Baba. Low-group-velocity and low-dispersion slow light in photonic crystal waveguides. *Opt. Lett.*, 32(20):2981–2983, Oct 2007. doi: 10.1364/OL.32.002981.
- [8] T. Baba. Slow light in photonic crystals. *Nature Photonics*, 2(8):465–473, Aug 2008. doi: 10.1038/nphoton.2008.146.
- [9] J. Shu and Y. Mao. Study of the properties of slow light in planar photonic crystal coupled-cavity waveguides. In *AOPC 2015: Advances in Laser Technology and Applications*, volume 9671, page 967100. SPIE, 2015. doi: 10.1117/12.2199249.
- [10] M. Notomi, K. Yamada, A. Shinya, J. Takahashi, C. Takahashi, and I. Yokohama. Extremely large group-velocity dispersion of line-defect waveguides in photonic crystal slabs. *Phys. Rev. Lett.*, 87:253902, Nov 2001. doi: 10.1103/PhysRevLett.87.253902.

- [11] K. Üstün and H. Kurt. Ultra slow light achievement in photonic crystals by merging coupled cavities with waveguides. *Opt. Express*, 18(20):21155–21161, Sep 2010. doi: 10.1364/OE.18.021155.
- [12] M. L. Povinelli, S. G. Johnson, and J. D. Joannopoulos. Slow-light, band-edge waveguides for tunable time delays. *Opt. Express*, 13(18):7145–7159, 2005. doi: 10.1364/OPEX.13.007145.
- [13] I. H. Giden, M. Turduev, and H. Kurt. Broadband super-collimation with low-symmetric photonic crystal. *Photonics and Nanostructures - Fundamentals and Applications*, 11(2):132–138, 2013. doi: <https://doi.org/10.1016/j.photonics.2012.12.001>.
- [14] J. Li, T. P. White, L. O’Faolain, A. Gomez-Iglesias, and T. F. Krauss. Systematic design of flat band slow light in photonic crystal waveguides. *Opt. Express*, 16(9):6227–6232, Apr 2008. doi: 10.1364/OE.16.006227.
- [15] M. Khatibi Moghaddam, A. R. Attari, and M. M. Mirsalehi. High coupling efficiency to a low dispersion slow light-supporting photonic crystal waveguide. *Journal of the European Optical Society - Rapid publications*, 8(0), 2013. ISSN 1990-2573. doi: 10.2971/jeos.2013.13066.
- [16] R. Hao, E. Cassan, H. Kurt, X. Le Roux, D. Marris-Morini, L. Vivien, H. Wu, Z. Zhou, and X. Zhang. Novel slow light waveguide with controllable delay-bandwidth product and ultra-low dispersion. *Opt. Express*, 18(6):5942–5950, Mar 2010. doi: 10.1364/OE.18.005942.
- [17] F. Bagci and B. Akaoglu. Enhancement of buffer capability in slow light photonic crystal waveguides with extended lattice constants. *Optical and Quantum Electronics*, 47(3):791–806, Mar 2015. doi: 10.1007/s11082-014-9953-8.
- [18] M. Danaie, A. Geravand, and S. Mohammadi. Photonic crystal double-coupled cavity waveguides and their application in design of slow-light delay lines. *Photonics and Nanostructures - Fundamentals and Applications*, 28:61–69, 2018. doi: <https://doi.org/10.1016/j.photonics.2017.11.009>.
- [19] S. A. Schulz, L. O’Faolain, D. M. Beggs, T. P. White, A. Melloni, and T. F. Krauss. Dispersion engineered slow light in photonic crystals: a comparison. *Journal of Optics*, 12(10):104004, Sep 2010. doi: 10.1088/2040-8978/12/10/104004.
- [20] L. He, Y. F. Gao, Z. Jiang, L. S. Wang, J. Zhou, and X. F. Xu. A unidirectional air waveguide basing on coupling of two self-guiding edge modes. *Optics & Laser*

Technology, 108:265–272, 2018. ISSN 0030-3992. doi: <https://doi.org/10.1016/j.optlastec.2018.06.044>.

- [21] M. K. Moghaddam and R. Fleury. Slow light engineering in resonant photonic crystal line-defect waveguides. *Opt. Express*, 27(18):26229–26238, Sep 2019. doi: 10.1364/OE.27.026229.
- [22] F. Shanhui and J. D. Joannopoulos. Analysis of guided resonances in photonic crystal slabs. *Phys. Rev. B*, 65:235112, Jun 2002. doi: 10.1103/PhysRevB.65.235112.
- [23] U. G. Yasa, M. Turduev, I. H. Giden, and H. Kurt. High extinction ratio polarization beam splitter design by low-symmetric photonic crystals. *J. Lightwave Technol.*, 35(9):1677–1683, May 2017. doi: 10.1109/JLT.2017.2657697.
- [24] M. A. Gumus, M. Tutgun, D. Yilmaz, and H. Kurt. A reduced symmetric 2d photonic crystal cavity with wavelength tunability. *Journal of Physics D: Applied Physics*, 52(32):325103, Jun 2019. doi: 10.1088/1361-6463/ab1f4b.
- [25] N. Erim, M. N. Erim, and H. Kurt. An optical sensor design using surface modes of low-symmetric photonic crystals. *IEEE Sensors Journal*, 19(14):5566–5573, Jul 2019. doi: 10.1109/JSEN.2019.2909863.
- [26] C. He, H. Wu, Y. Feng, W. Su, and F. Li. Dynamic modulation of slow light rainbow trapping and releasing in a tapered waveguide based on low-symmetric photonic crystals. *Results in Physics*, 28:104592, 2021. doi: 10.1016/j.rinp.2021.104592.
- [27] J. Vucic, M. Loncar, H. Mabuchi, and A. Scherer. Design of photonic crystal microcavities for cavity qed. *Phys. Rev. E*, 65:016608, Dec 2001. doi: 10.1103/PhysRevE.65.016608.
- [28] Y. Gao, L. He, Z. Jiang, J. Zhou, Y. Shi, and W. Bai. Investigation of coupling effect between a unidirectional air waveguide and two cavities with one-way rotating state. *Optica Applicata*, Vol. 50, nr 1:49–59, 2020. doi: 10.37190/oa200104.
- [29] R. Yang, W. Zhu, and J. Li. Realization of “trapped rainbow” in 1d slab waveguide with surface dispersion engineering. *Opt. Express*, 23(5):6326–6335, Mar 2015. doi: 10.1364/OE.23.006326.
- [30] Y. F. Gao, M. Zhou, and W. Zhang. Novel dispersion properties of one-dimensional photonic crystals containing a defect made of twin prisms. *Journal of Russian Laser Research*, 33(3):211–216, May 2012. ISSN 1573-8760. doi: 10.1007/s10946-012-9274-y.

- [31] K. L. Tsakmakidis, A. D. Boardman, and O. Hess. ‘trapped rainbow’ storage of light in metamaterials. *Nature*, 450(7168):397–401, Nov 2007. ISSN 1476-4687. doi: 10.1038/nature06285.
- [32] Q. Gan, Y. J. Ding, and F. J. Bartoli. “rainbow” trapping and releasing at telecommunication wavelengths. *Phys. Rev. Lett.*, 102:056801, Feb 2009. doi: 10.1103/PhysRevLett.102.056801.
- [33] Y. Liu, Y. Wang, G. Han, Y. Shao, C. Fang, S. Zhang, Y. Huang, J. Zhang, and Y. Hao. Engineering rainbow trapping and releasing in ultrathin thz plasmonic graded metallic grating strip with thermo-optic material. *Opt. Express*, 25(2):1278–1287, Jan 2017. doi: 10.1364/OE.25.001278.
- [34] Y. Liu, R. Kanyang, G. Han, Y. Shao, C. Fang, Y. Huang, S. Zhang, J. Zhang, and Y. Hao. Rainbow trapping in highly doped silicon graded grating strip at the terahertz range. *IEEE Photonics Journal*, 10(3):1–9, 2018. doi: 10.1109/JPHOT.2018.2816566.
- [35] A. Arreola-Lucas, G. Báez, F. Cervera, A. Climente, R. A. Méndez-Sánchez, and J. Sánchez-Dehesa. Experimental evidence of rainbow trapping and bloch oscillations of torsional waves in chirped metallic beams. *Scientific Reports*, 9:1860, 2019. doi: 10.1038/s41598-018-37842-7.
- [36] B. Neşeli, E. Bor, H. Kurt, and M. Turduev. Rainbow trapping in a tapered photonic crystal waveguide and its application in wavelength demultiplexing effect. *J. Opt. Soc. Am. B*, 37(5):1249–1256, 2020. doi: 10.1364/JOSAB.388374.
- [37] P. Ghaderian and A. Habibzadeh-Sharif. Rainbow trapping and releasing in graded grating graphene plasmonic waveguides. *Opt. Express*, 29(3):3996–4009, 2021. doi: 10.1364/OE.414982.
- [38] Z. Hayran, M. Turduev, M. Botey, R. Herrero, K. Staliunas, and H. Kurt. Numerical and experimental demonstration of a wavelength demultiplexer design by point-defect cavity coupled to a tapered photonic crystal waveguide. *Opt. Lett.*, 41(1):119–122, Jan 2016. doi: 10.1364/OL.41.000119.
- [39] S. G. Johnson and J. D. Joannopoulos. Block-iterative frequency-domain methods for maxwell’s equations in a planewave basis. *Opt. Express*, 8(3):173–190, 2001. doi: 10.1364/oe.8.000173.
- [40] A. Taflove and S. C. Hagness. *Computational Electrodynamics: The Finite-Difference Time-Domain Method*. Artech House, Norwood, 3rd edition, 2005. doi: 10.1016/B978-012170960-0/50046-3.

- [41] A. F. Oskooi, D. Roundy, M. Ibanescu, P. Bermel, J. D. Joannopoulos, and S. G. Johnson. Meep: A flexible free-software package for electromagnetic simulations by the fdtd method. *Comput. Phys. Commun.*, 181(3):687–702, 2010. ISSN 0010-4655. doi: 10.1016/j.cpc.2009.11.008.
- [42] J. M. Liu. *Photonic Devices*. Cambridge University Press, 2005. ISBN 9780511614255. doi: 10.1017/CBO9780511614255.
- [43] J. K. S. Poon, J. Scheuer, Y. Xu, and A. Yariv. Designing coupled-resonator optical waveguide delay lines. *J. Opt. Soc. Am. B*, 21(9):1665–1673, Sep 2004. doi: 10.1364/JOSAB.21.001665.
- [44] T. Baba, J. Adachi, N. Ishikura, Y. Hamachi, H. Sasaki, T. Kawasaki, and D. Mori. Dispersion-controlled slow light in photonic crystal waveguides. *Proceedings of the Japan Academy. Series B, Physical and biological sciences*, 85(10):443–453, 2009. doi: 10.2183/pjab.85.443.
- [45] Z. M. Yuksel, H. Oguz, O. O. Karakilinc, M. Turduev, H. Berberoglu, M. Adak, and S. Ozdemir Kart. Enhanced self-collimation effect by low rotational symmetry in hexagonal lattice photonic crystals. *Physica Scripta*, 99(6):065017, may 2024. doi: 10.1088/1402-4896/ad4426.
- [46] R. J. P. Engelen, Y. Sugimoto, Y. Watanabe, J. P. Korterik, N. Ikeda, N. F. van Hulst, K. Asakawa, and L. Kuipers. The effect of higher-order dispersion on slow light propagation in photonic crystal waveguides. *Optics Express*, 14(4):1658–1672, 2006. doi: 10.1364/OE.14.001658.
- [47] H. Hu, D. Ji, X. Zeng, K. Liu, and Q. Gan. Rainbow trapping in hyperbolic metamaterial waveguide. *Scientific Reports*, 3(1):1249, Feb 2013. doi: 10.1038/srep01249.